Anal. Chem. **2002,** *74,* 4895−4904

Bacteria Sorting by Field-Flow Fractionation. Application to Whole-Cell *Escherichia coli* Vaccine Strains

Pierluigi Reschiglian,* Andrea Zattoni, Barbara Roda, and Sonia Casolari

Department of Chemistry "G. Ciamician", University of Bologna, Via Selmi 2, I-40126 Bologna, Italy

Myeong Hee Moon, Jisun Lee, and Jaehong Jung

Department of Chemistry, Pusan National University, Pusan 609-735, Korea

Kåre Rodmalm†

SBL Vaccin AB, SE-10521 Solna, Sweden

Giovanna Cenacchi

Clinical Department of Radiology and Histopathology, Via Massarenti 9, I-40138 Bologna, Italy

Sorting and quantification of deactivated bacteria is an important way of quality control for whole-cell bacterial vaccines. In general, surface features of deactivated bacteria used for whole-cell bacterial vaccines affect the immunoresponse to bacteria-associated antigens. Enumeration of bacteria is also an important process development parameter for these vaccines. Field-flow fractionation (FFF) was previously applied to the separation of bacteria. For the first time, FFF is used for sorting bacteria strains of the same species on the basis of differences in bacterial membrane characteristics. Two FFF techniques, gravitational FFF (GrFFF) and asymmetrical flow FFF (AsFlFFF), are shown to be able to fractionate, distinguish, and quantify different deactivated *Escherichia coli* strains used for vaccines. *E. coli* can differ in the presence of fimbriae on the bacterial membrane. Fimbriae affect *E. coli* pathology and thus the use of *E. coli* for vaccines. GrFFF and AsFlFFF are able to fractionate fimbriated/nonfimbriated cells in mixtures of different strains. While GrFFF is characterized by low cost and simplicity, AsFlFFF shows a higher performance in size fractionation with a high-speed separation. Coupled, on-line UV/visible turbidimetry yields the relative numbers of fractionated cells and sample recovery. Scanning electron microscopy and quasi-elastic light scattering are employed as uncorrelated techniques for size and morphology analysis of the *E. coli* strains.

Over more than a decade, field-flow fractionation (FFF) has shown to be well-suited for the selection of bacteria. In particular, a specifically designed variant of FFF was shown able to select *Escherichia coli* mutants on the basis of motility differences.[1] Classical sedimentation field-flow fractionation (SdFFF) of flagellated and nonflagellated *E. coli* strains was then shown by Giddings as an example of FFF for biological applications.[2] Flagellated and nonflagellated *E. coli* therein confirmed different elution behavior and, thus, a sufficiently different retention time to be distinguished by SdFFF since motile bacteria contributed differently to retention. Differences in motility between live and dead bacteria were further confirmed to give different elution profiles in SdFFF and flow field-flow fractionation (FlFFF).[3] Hollow fiber flow field-flow fractionation (HF FlFFF) has recently shown to be able to fractionate deactivated *Vibrio cholerae* for whole-cell bacterial vaccines.[4]

Vaccines based on deactivated bacteria are of broad use for immunoprophylaxis against many diseases that are caused by or related to bacterial infections. Because of the often mandatory immunoprophylaxis required for tourists visiting tropical and subtropical areas, production of highly purified, efficient vaccines with negligible side effects is also important. Furthermore, the emerging threat of biological warfare is a dramatic reminder of the possible needs of massive vaccination campaigns. For more than two decades, *E. coli* has been a workhorse of biotechnology because of its broad use in cloning and gene engineering techniques. These bacteria form part of the natural human gastrointestinal tract flora. However, they can often cause common infections, e.g., urinary tract bacteriuria or traveler's dysentery. Moreover, highly pathogenic *E. coli* strains are known to be the cause of outbreaks associated with undercooked and contaminated ground beef, which were responsible for many deaths in the early

* Corresponding author. Phone: +39(0)512099564. Fax: +39(0)512099456. E-mail: resky@ciam.unibo.it.

† Current address: AB Ninolab, Box 137, 194 22 Upplands Väsby, Sweden.

(1) Berg, H. C.; Turner, L. *Proc. Natl. Acad. Sci. U.S.A.* **1991**, *88*, 8145−8148.
(2) Giddings, J. C. *Science* **1993**, *260*, 1456−1465.
(3) Saenton, S.; Lee, H. K.; Gao, Y.; Ranville J.; Ratanathanawongs Williams, S. K. *Sep. Sci. Technol.* **2000**, *35*, 1761−1775.
(4) Reschiglian, P.; Roda, B.; Zattoni, A.; Min, B.-R.; Moon, M.-H. *J. Sep. Sci.* **2002**, *25*, 490−498.

10.1021/ac020199t CCC: $22.00
Published on Web 08/31/2002

1990s. Immunoprophylaxis directed against infections caused by pathogenic *E. coli* variants has thus received increased interest. Production of deactivated strains for whole-cell *E. coli* vaccines is emerging in biotechnology. Consequently, the need for methods of quality assessment and process control of the complete productive cycle is growing. It is known that *E. coli* motility and surface features can affect pathogenicity and immunoresponse to *E. coli*-assisted antigens. The presence of flagellae is also known to influence not only *E. coli* motility but also their adhesion properties. *E. coli* without flagellae can also differ with regard to the presence of fimbriae, rod-shaped proteinaceous protrusions on the bacterial surface. Fimbriae are a large and heterogeneous family. Most fimbriae are made up of small (10−15 kDa) protein monomers, "building blocks" that form the rods. The molecular mass of the assembled structures can reach several million daltons. Fimbriated and nonfimbriated *E. coli* adhere differently to target tissues. Fimbriae actually are colonization factors used by *E. coli* to adhere to epithelial cells in the human gut.[5] Consequently, the expression of fimbriae in vaccine strains is crucial to the efficacy of whole-cell *E. coli* vaccines. The use of deactivated, fimbriated *E. coli* can actually allow vaccinated patients later exposed to live, pathogenic *E. coli* to produce antifimbrial antibodies that block the adhesion of *E. coli* and thus inhibit colonization. Evaluation of the presence of fimbriae, and quantitation of fimbriated *E. coli* cells in bulk suspensions and final vaccines, can therefore be a fundamental aspect in quality and process control of whole-cell *E. coli* vaccine production.

In this work, gravitational FFF (GrFFF) and the asymmetrical variant of FlFFF (AsFlFFF) are for the first time employed to sort and quantify fimbriated and nonfimbriated, deactivated *E. coli* strains used for whole-cell vaccines. Although GrFFF was sometimes thought of as the modest member of the FFF family, it has already been proved highly suitable for the separation and further characterization of different types of cells at a high sample recovery.[6−16] GrFFF employs Earth's gravitational field applied perpendicularly to a very thin, empty channel. This is the first time GrFFF has been shown to also be able to fractionate small, low-density bacteria. FlFFF is the most versatile member of the FFF family. AsFlFFF employs only one permeable wall (the accumulation wall) to allow part of the mobile phase flowing inside the channel to go through the accumulation wall and generate the hydrodynamic, perpendicular field that develops separation.[17,18] Different fimbriated and nonfimbriated, deactivated *E. coli* strains were analyzed by GrFFF and AsFlFFF, and both studies gave distinguishable profiles with different retention times. Scanning electron microscopy (SEM) and quasi-elastic light scattering (QELS) are allowed to eventually assess whether differences in retention between the strains were due to differences in size and shape or rather caused by the presence of fimbriae on the *E. coli* membrane. Coupled UV/visible turbidity was proved to be suitable for quantitative analysis. Correlation between UV/visible detector signal and number of cells was obtained and the limit of detection for *E. coli* in GrFFF−UV/visible spectroscopy was thereby determined. Sample mixtures of fimbriated and nonfimbriated cells always provided double-band FFF fractograms with different band areas that quantitatively corresponded to different fimbriated/nonfimbriated cell ratio values in the injected sample mixtures. Highly selective AsFlFFF is allowed to sort both cell types at very short analysis times with a baseline resolution separation of such mixtures of different *E. coli* strains. AsFlFFF showed a high selectivity in the size-based fractionation of *E. coli* cells. All these findings open up interesting perspectives for the application of FFF−UV/visible spectroscopy methods for quick sorting and quantification of bacteria.

EXPERIMENTAL SECTION

GrFFF System. The GrFFF system, employed here, was assembled as described recently.[16,19] The depletion wall was made of polycarbonate (PC) and the accumulation wall of poly(vinyl chloride) (PVC). This new channel design was specifically developed for the fractionation of cells and samples of natural origin. Plastic walls in GrFFF and SdFFF had already been successfully proposed for the fractionation of cells, because of reduced cell wall interactions and higher biocompatibility.[20] Nominal channel dimensions were as follows: 30.0 cm (tip-to-tip length), 2.5 cm (tapered ends length), 2.0 cm (breadth), 0.0180 cm (thickness), 55.0 cm^2 (channel surface). These corresponded to a nominal channel volume of 0.99 cm^3. The experimental channel volume was determined by injecting an unretained probe ($K_2Cr_2O_7$) at a flow rate of 0.4 mL min^{-1} and resulted in 1.05 ± 0.01 mL. This value corresponded to an experimental channel thickness of 0.0191 ± 0.0007 cm.

The GrFFF channel was installed in two different laboratories. It simply replaced the column in either a HPLC Workstation BioCAD SPRINT System (Perseptive Biosystems, Inc., Framingham, MA), or in a model 2510/2550 HPLC Workstation (Varian, Palo Alto, CA). In both systems, the injection port was the valve Rheodyne model 7125 (Rheodyne, Cotati, CA) with a 20-μL loop. The inlet tube was glued either at the depletion or at the accumulation wall of the channel to allow a choice between "up-bottom" or "bottom-up" sample injection.

AsFlFFF System. The AsFlFFF system employed was home-built using Plexiglas blocks. The channel had only one permeable wall (accumulation wall) that was built in one of the Plexiglas

(5) Nataro, J. P.; Kaper, J. B. *Clin. Microbiol. Rev.* **1998**, *11*, 142−201.
(6) Cardot, P. J. P.; Gerota, J.; Martin, M. *J. Chromatogr.* **1991**, *568*, 93−103.
(7) Merino-Dugay, A.; Cardot, Ph. J. P.; Czok, M.; Guernet, M.; Andreux, J. P. *J. Chromatogr.* **1992**, *579*, 73−83.
(8) Urbánková, E.; Vacek, A.; Nováková, N.; Matulík, F.; Chmelík, J. *J. Chromatogr.* **1992** *583*, 27−34.
(9) Plocek, J.; Konecný, P.; Chmelík, J. *J. Chromatogr., B* **1994**, *656*, 427−431.
(10) Cardot, P. J. P.; Elgea, C.; Guernet, M.; Godet, D.; Andreux, J. P. *J. Chromatogr., B* **1994**, *654*, 193−203.
(11) Bernard, A.; Paulet, B.; Colin, V.; Cardot, Ph. J. P. *TrAC, Trends Anal. Chem.* **1995**, *14*, 266−273.
(12) Urbánková, E.; Vacek, A.; Chmelík, J. *J. Chromatogr., B* **1996**, *687*, 449−452.
(13) Cardot, P. J. P.; Launay, J. M.; Martin, M. *J. Liq. Chromatogr. Relat. Technol.* **1997**, *20*, 2543−2553.
(14) Lucas, A.; Lepage, F.; Cardot, P. In *Field-Flow Fractionation Handbook*; Schimpf, M. E., Caldwell, K., Giddings, J. C., Eds.; Wiley-Interscience: New York, 2000; Chapter 29.
(15) Sanz, R.; Puignou, L.; Reschiglian, P.; Galceran, M. T. *J. Chromatogr., A* **2001**, *919*, 339−347.
(16) Sanz, R.; Torsello, B.; Reschiglian, P.; Puignou, L.; Galceran, M. T. *J. Chromatogr., A* **2002**, *966*, 135−143.
(17) Wahlund, K.-G.; Giddings, J. C. *Anal. Chem.* **1987**, *59*, 1332−1339.
(18) Litzen, A.; Wahlund, K.-G. *Anal. Chem.* **1991**, *63*, 1001−1007.
(19) Reschiglian, P.; Zattoni, A.; Casolari, S.; Chmelík, J.; Krumlova A.; Budinska, M. *Ann. Chim. (Rome)* **2002**, *92*, 457−467.
(20) Chiana, T.; Cardot, Ph. J. P.; Assidjo, A.; Monteil, J.; Clarot, I.; Krausz, P. *J. Chromatogr., B* **1999**, *734*, 91−99.

blocks using a ceramic frit. The other wall (depletion wall) was made by the other Plexiglas block that had been drilled with three holes for carrier inlet, sample inlet, and sample outlet. The channel was cut out from a Mylar thin sheet (130-μm thickness) and sandwiched between the Plexiglas blocks with a sheet of PLGC (regenerated cellulose) membrane (Millipore Corp., Bedford, MA) of 10-kDa cutoff, which was layered above the accumulation wall. The membrane kept sample components from possible penetration through the ceramic frit. The AsFlFFF channel had a tip-to-tip length of 27.2 cm and a breadth of 2.0 cm with triangular end pieces at both ends. Mobile phase was delivered by means of two HPLC pumps (model LC-10AD) from Shimadzu (Kyoto, Japan): one was employed for sample introduction and the other for its separation. Sample injection was made with a model 7125 loop injector from Rheodyne equipped with a 20-μL loop. Eluted sample components were monitored with a model M720 UV detector from Young-Lin Co. (Seoul, Korea) at a wavelength of 254 nm. Detector signal was handled by AutochroWin, data acquisition software from Young-Lin Co.

Samples and Mobile Phases. Three different samples of deactivated *E. coli* from SBL Vaccin AB were analyzed: two CS5 strains, one fimbriated (batch 0398) and one that had been cultivated at conditions inhibiting fimbriae formation (batch 001101-5), and a nonfimbriated strain used as vaccine placebo (batch XC113A2). All these strains were originally suspended in PBS buffer with added 0.02% NaN_3 (w/v). Turbidity measurements for the evaluation of the number of cells in the *E. coli* batches were performed on a reference benchtop UV/visible SECOMAM spectrophotometer (Domont, France). The spectrophotometer was calibrated at 600-nm wavelength with the reference *E. coli* strain CFA/1 $OD_{600} = 53$ (from SBL Vaccin).

Standard, NIST-traceable polystyrene latex spheres (PS) from Duke Scientific (Palo Alto, CA) were employed to determine the AsFlFFF size-based selectivity before fractionation of *E. coli*. PS had mean diameters of 6.995, 4.991, 4.000, 3.004, and 2.013 μm (hereafter designated 7, 5, 4, 3, and 2 μm). The nominal, solid contents of PS ranged 0.30−0.50% (w/v). Injection of PS standard was made of about 1−3 μL of nondiluted PS suspensions. They were sequentially sampled with a syringe for HPLC and loaded into the injector port for a simultaneous injection into the AsFlFFF channel.

For comparing AsFlFFF retention of PS and *E. coli*, an aqueous solution of 0.1% (v/v) FL-70 (Fisher Scientific Co., Fairlawn, NJ), a surfactant mixture made of 3.0% oleic acid, 3.0% Na_2CO_3, 1.8% Tergitol, 1.4% tetrasodium ethylenediamine tetraacetate, and 1.0% poly(ethylene glycol) 400 in water, was added with 0.01% NaN_3 and used as mobile phase. A mobile phase for the separation of *E. coli* by both GrFFF and AsFlFFF was made by mixing 80% (v/v) Milli-Q water (Millipore), added with 0.05% (w/v) sodium dodecyl sulfate (SDS) and 0.01% (w/v) NaN_3, with 20% (v/v) HPLC-grade methanol (MeOH).

GrFFF Operations. *E. coli* samples were always kept at 4 °C. When stored overnight, they were ultrasound stirred for 3 min in order to prevent aggregation. They were then vortexed for ∼30 s before the injection, which was performed at 0.2 mL min^{-1} for 15−25 s. Flow was then stopped to allow for sample relaxation. The relaxation time ranged from 15 to 30 min. After relaxation, flow was restored at the chosen elution flow rate.

AsFlFFF Operations. Sample relaxation was achieved by using the focusing/relaxation method, in which two different carrier streams entered through both the inlet and outlet of the channel, and relevant flow rates were adjusted to focus sample at a given position inside the channel. The sample focusing position was visually set at 2.7 cm downstream from the channel inlet by injecting a dye. Sample injection was made at 0.2 mL min^{-1} while focusing flow streams were entering the channel. After 45 s of sample injection, the flow was diverted to waste and the focusing/relaxation step begun. The focusing/relaxation flow rate was kept constant for all runs and equal in value to the sum of the outflow (V_{out}) and the cross-flow (V_{cross}) rate. Once relaxation had reached completion (i.e., after ∼45 s), the focusing flow stream entering through the channel outlet was reversed toward the channel inlet for the separation step. Flow conversion was done via one four-way and one three-way valve. Valve configurations for sample injection, focusing/relaxation, and elution modes were similar to that described in the literature.[21]

SEM of *E. coli*. Dispersed *E. coli* batch samples were fixed by adding at least 10 mL of 1% glutaraldehyde in 0.1 M cacodylate buffer. After a 3-h fixation, the bacteria were washed in 0.15 M cacodylate buffer and seeded on poly(L-lysine)-coated glass coverslips in a moist chamber. The coverslips were stored overnight at 4 °C, washed in the same buffer, and postfixed for 1 h in 1% osmium tetroxide. After dehydration in a graded series of ethanol solutions, the specimens were critical point dried, mounted on aluminum stubs, sputtered with gold, and examined with a Philips model 505 SEM (Philips Analytical, Natick, MA). Microscopic examination was performed at 20 kV and an angle of 30°.

SEM sizing of *E. coli* fractions collected from AsFlFFF runs was made by a model S-4200 field emission SEM (FE SEM) from Hitachi Ltd. (Tokyo, Japan). Collected fractions of nonfimbriated *E. coli* cells were spotted on polycarbonate membrane having pore sizes of 0.4 μm in diameter and dried. In the case of fimbriated *E. coli* fractions, due to the cell rupture upon air-drying, specimens were fixed with 1% osmium tetroxide and followed by dehydration with ethanol and isoamyl acetate. The so-treated cells were filtered onto a 13-mm polycarbonate membrane, and the critical point drying procedure was then applied. Then the membrane was fixed over a copper stub by using graphite colloid glue and sputtered with Pt for 120 s. Microscopic examination was performed at 15 kV and an angle of 0°.

QELS of *E. coli*. QELS size analysis was performed by using a 90Plus Particle Sizer (Brookhaven Instruments Corp., Holtsville, NY). Before analysis, batch samples were diluted 1:1000 to obtain a concentration of $\sim 10^4$ cells mL^{-1} and then allowed to equilibrate for at least 15 min. The sample holder was a quartz, 1-cm path length cuvette for spectrofluorometry. The incident radiation was set at 532.0-nm wavelength. The scattered light was read at 90° from the direction of the incident beam. The instrument software (90Plus Particle Sizing Software Ver. 2.31) gave the values of sample effective diameter and half-width of the size distribution, all expressed as mean values from three runs of 2 min each. Sample temperature was kept constant at 37.0 °C, and a viscosity of 0.692 cP was assumed for all samples. A software dust filter for particles larger than 10 μm was employed in all cases.

(21) Lee, W. J.; Min, B.-R.; Moon, M. H. *Anal. Chem.* **1999**, *71*, 3446−3452.

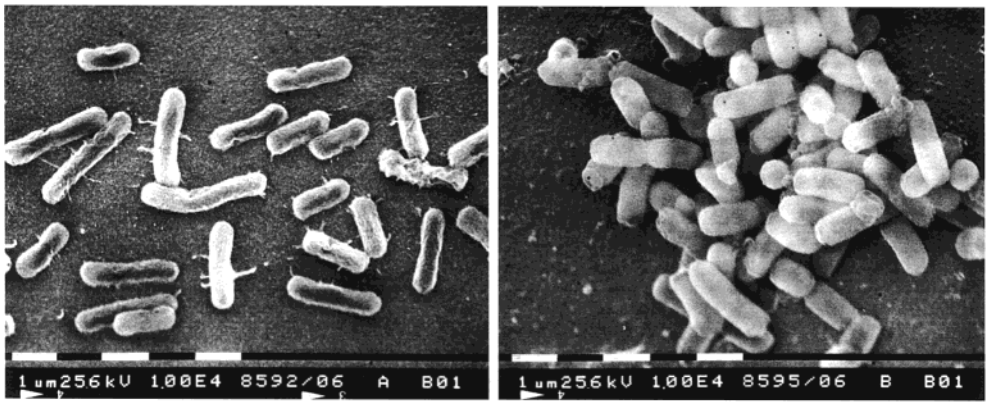

Figure 1. SEM pictures of *E. coli* batch samples: (a) fimbriated CS5 0398; (b) nonfimbriated CS5 001101-5.

Table 1. QELS Sizing of *E. coli* Strains

strain	fimbriated CS5 0398		nonfimbriated CS5 001101-5	
carrier	PBS	SDS/NaN_3/MeOH 20%	PBS	SDS/NaN_3/MeOH 20%
effective diameter (nm)	2426 ± 182	1444 ± 34	1870 ± 462	1116 ± 113
half-width (nm)	605 ± 441	902 ± 25	320 ± 135	685 ± 95

RESULTS AND DISCUSSION

Figure 1 respectively shows SEM pictures of the CS5-fimbriated cells (batch 0398) and of the CS5 cells grown under conditions inhibiting fimbriae formation (batch 001101-5). *E. coli* appears rod-shaped with fimbriated cells showing "pili" on the membrane. In all the microscopy fields taken, SEM shows the presence of pili in all the CS5-fimbriated cells (Figure 1a) and the total absence of these pili in all the CS5 cells that were grown under conditions to inhibit fimbriae formation (Figure 1b). As expected, the size and shape of *E. coli* cells appear not to be different for the two CS5 strains. Since *E. coli* cells are not spherical, definition of size is not a trivial issue. In most real cases of irregular particles, the size can actually be expressed in terms of a sphere equivalent to the particle with regard to some properties. The hydrodynamic radius can be taken as an estimation of the size of such rod-shaped cells. QELS (otherwise called photon correlation spectroscopy, PCS) is a well-established technique for measuring the hydrodynamic radius of particles.[22] In Table 1, it is reported that the hydrodynamic radius values are determined by QELS for the same CS5 fimbriated (batch 0398) and CS5 nonfimbriated cells (batch 001101−5) of Figure 1. To also establish whether size could be affected by the composition of the dispersing agent used in the mobile phase, samples were suspended either in PBS (the original suspending medium for *E. coli* batch samples) or in the mobile phase used commonly in GrFFF and AsFlFFF of *E. coli* (0.05% SDS/0.01% NaN_3/20% MeOH). In Table 1, one can observe some differences in the size values obtained by QELS, either when any strain was suspended in different dispersing media or when the two strains were suspended in the same medium. One must recall that retention in GrFFF and AsFlFFF is considered to depend, first, on sample size. It is generally known that there are two possible elution modes in FFF, each given by different retention mechanisms. A rational approach for distinguishing elution modes and retention mechanisms has been recently worked out by Wahlund and Zattoni.[23,24] The definition of normal and reversed mode therein proposed has retained the definition of classical liquid chromatography, whereas in FFF, it refers only to the elution order. In normal FFF mode, smaller particles actually elute first while they elute last in reversed FFF mode. The conditions at which transition between the two elution modes occurs for ideal, spherical particles was reported in fundamental FFF literature.[25] In GrFFF, the transition from normal to reversed mode occurs to particles in the micronsize range and it also depends on particle density. In AsFlFFF, the transition depends also on the applied flow rates but it is independent of particle density. Because of the measured micrometer-size, hydrodynamic diameter values of *E. coli* reported in Table 1, elution of *E. coli* is then expected to be reversed in both GrFFF and AsFlFFF. In reversed FFF, the retention mechanism can be steric (St), steric/hyperlayer (St/Hyp), or hyperlayer (Hyp) (otherwise called "focusing"[26]), and it can be studied by measuring the size-based selectivity.

GrFFF of *E. coli*. Figure 2 shows a few examples of fractograms obtained for different *E. coli* strains. It is evident that GrFFF profiles for the fimbriated strain (Figure 2a) are very different from fractograms of the nonfimbriated strains (Figure 2b and c). Reproducibility can be observed in all cases. Possible bacterial aggregation before injection was excluded by optical microscopy on fresh samples. This confirmed that differences between fractograms were not caused by experimental artifacts. Injection was performed bottom-up with relaxation time set at 15 min. The presence in all fractograms of Figure 2 of a very intense void band, with poor resolution between void and sample bands, is evident. This finding would indeed suggest the need for longer stop-flow time to increase sample relaxation, although the bottom-up injection design has been adopted to drastically reduce

(22) Weiner, B. B. In *Modern Methods of Particle Size Analysis*; Barth, H. G., Ed.; Wiley-Interscience: New York, 1984; Chapter 3, pp 93−116.

(23) Wahlund, K.-G.; Zattoni, A. *Anal. Chem.*, in press (AC020315S).

(24) Wahlund, K.-G.; Zattoni, A. *FFF2001, 9th Int. Symp. on Field-Flow Fractionation*, June 26−29, 2001, Abstract Book, Communication L1.

(25) Caldwell, K. In *Field-Flow Fractionation Handbook*; Schimpf, M. E., Caldwell, K., Giddings, J. C., Eds.; Wiley-Interscience: New York, 2000; Chapter 5, p 79.

(26) Martin, M.; Williams, P. S. In *Theoretical Advancement in Chromatography and Related Separation Techniques*; Dondi, F., Guichon, G., Eds.; NATO ASI Series; Kluwer Academic Publishers: Dordrecht, The Netherlands, 1982; p 547.

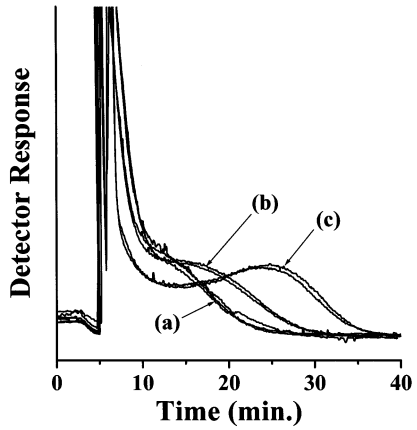

Figure 2. GrFFF of *E. coli*. Elution flow rate, 0.3 mL min^{-1}; injection design bottom-up; stop-flow time, 15 min. (a) Fimbriated CS5 0398; (b) nonfimbriated XC113A2; (c) nonfimbriated CS5 001101-5. Repeated runs reported for each case.

relaxation time.[11] A long stop-flow period, in fact, not only increments the total analysis time but it can also reduce sample recovery, because of the longer period of static permanence of the sample inside the channel. However, 20% MeOH (v/v) in the mobile phase was employed in all these GrFFF experiments. The presence of MeOH does not affect biocompatibility, due to *E. coli* samples being deactivated. Such a MeOH percentage has been shown successful for GrFFF of yeast cells because the use of an organic modifier can reduce the extent of electrostatic interactions between cells and channel walls.[15,16] Otherwise, the presence of MeOH dramatically increases the mobile-phase viscosity (at 20 °C, $\eta = 1.604$ cP for the 20% MeOH/80% H_2O binary mixture, $\eta = 1.002$ cP for pure H_2O), which can thus make the required relaxation process longer than with aqueous media. In Figure 3a and b, the fractograms of the CS5 fimbriated 0398 and the CS5 nonfimbriated 001101-5 samples are obtained by increasing stop-flow time to 30 min. Other analysis conditions were the same as in Figure 2. If fractograms in Figure 3 and Figure 2 are compared, it is clear that the increase in stop-flow time led to a more complete sample relaxation and, consequently, to a better resolution between void and sample bands. A reduction of void peak amplitude is also observed. Fractograms in Figure 3 were obtained either by injecting bottom-up or up-bottom. If one refers to fractograms in Figure 2, which were obtained with a 15-min stop-flow after bottom-up injection, fractograms in Figure 3 might indicate that, with the use of a loop valve as injection port and with such a MeOH-added mobile phase, the relaxation process of *E. coli* might be relatively independent of the injection design. However, more insights into this specific, instrumental topic stands beyond the aims of the present paper. In Figure 3a, fractograms obtained at different loads of the same fimbriated strain (CS5 0398) are compared. It is confirmed that, in GrFFF, sample overloading tends to shift retention times to a shorter time scale.[27] In Figure 3b, fractograms obtained for the same nonfimbriated strain (CS5 001101-5) at different flow rates are compared. For better comparison, fractograms are reported as a function of $1/R$ (where $R = t_0/t_r$, with t_0 and t_r the void and the retention time, respectively). Retention tends to be reduced with increasing flow rate, due to the effect of flow rate-dependent hydrodynamic forces.[26]

Fractograms in Figures 2 and 3 and QELS data in Table 1 indicate that the great separation observed between fimbriated and nonfimbriated cells cannot be based on size differences only. The "anomalous" retention behavior and the possible effects of variables other than size in reversed FFF were in fact observed by Caldwell et al. since early GrFFF[28] and further confirmed in their pioneering report on FFF of cells.[29] In reversed GrFFF of cells under defined analysis conditions, retention was then found by Cardot et al. to depend also on density, shape, flexibility, particle surface chemistry, and their relevant distributions within the sample. These multiple polydispersity indexes are now called the "polydispersity matrix".[14] All these factors other than size have already been experimentally observed to modulate GrFFF retention of red blood cells,[30] stem cells,[12] and most recently yeast cells.[15,16] Otherwise it is known that *E. coli* surface properties including hydrophobicity, surface free energy, surface charge, and ζ-potential can influence their interaction to solid surfaces.[31] These interactive forces come into play to different extents between fimbriated/nonfimbriated *E. coli* cells and plastic walls, and they could give rise to the onset of *E. coli* cell wall interaction able to modulate GrFFF retention.[32] On the other hand, the presence of fimbriae can induce differences in cell flexibility which, for rod-shaped particles, have recently been demonstrated to induce differences in hydrodynamic forces able to modify FFF retention.[33] Last, but not least, differences in density between fimbriated and nonfimbriated cells cannot be excluded as a priori. Correlation between GrFFF retention and *E. coli* features can thus be hard to achieve. FlFFF is, in principle, independent of particle density and particularly well suited to exploit flow rate-dependent hydrodynamic forces in reversed mode.[34,35] Reversed AsFlFFF may be able to confirm whether differences in retention between fimbriated and nonfimbriated *E. coli* could be due to factors other than size.

Quantification of Sorted *E. coli* Cells. To quantify sorted *E. coli* cells, on-line UV/visible turbidity is used as it was first reported for SdFFF of bacteria.[36] For more accurate results, calibration of the injection valve loop and detector cell path length is performed in the present work, according to the methodology described elsewhere.[37] Actual loop volume and cell path length were so measured to be $V_{loop} = 22.6 \pm 0.4$ μL ($N = 12$) and $b = 0.613 \pm 0.002$ cm ($N = 12$), respectively. A reference benchtop spectrophotomer was then used to determine the number of cells in the *E. coli* batch samples. The reference benchtop spectropho-

(27) Pazourek, J.; Chmelík, J. *J. Chromatogr., A* **1995**, *715*, 259−265.
(28) Caldwell, K. D.; Nguyen, T. T.; Myers, M. N.; Giddings, J. C. *Sep. Sci. Technol.* **1979**, *14*, 935−946.
(29) Caldwell, K. D.; Cheng, Z. Q.; Hradecky, P.; Giddings, J. C. *Cell Biophys.* **1984**, *6*, 233−251.
(30) Parsons, R.; Yue, V.; Tong, X.; Cardot, Ph.; Bernard, A.; Andreux, J. P.; Caldwell, K. *J. Chromatogr., B* **1996**, *686*, 177−187.
(31) Harkes, G.; Feijen, J.; Dankert, J. *Biomaterials* **1991**, *12*, 853−860.
(32) Reschiglian, P.; Melucci, D.; Torsi, G. *J. Chromatogr., A* **1996**, *740*, 245−252.
(33) Zhao, Y.; Sharp, M. K. *J. Biomech. Eng.* **1999**, *121*, 148−152.
(34) Ratanathanawongs, S. K.; Giddings, J. C. *Anal. Chem.* **1982**, *64*, 6−15.
(35) Reschiglian P.; Melucci, D.; Zattoni, A.; Malló, L.; Hansen, M.; Kummerow, A.; Miller, M. *Anal. Chem.* **2000**, *72*, 5945−5954.
(36) Sharma, R. V.; Edwards, R. T.; Beckett, R. *Appl. Environ. Microb.* **1993**, *59*, 1864−1875.
(37) Reschiglian, P.; Melucci, D.; Torsi, G. *Chromatographia* **1997**, *44*, 172−178.

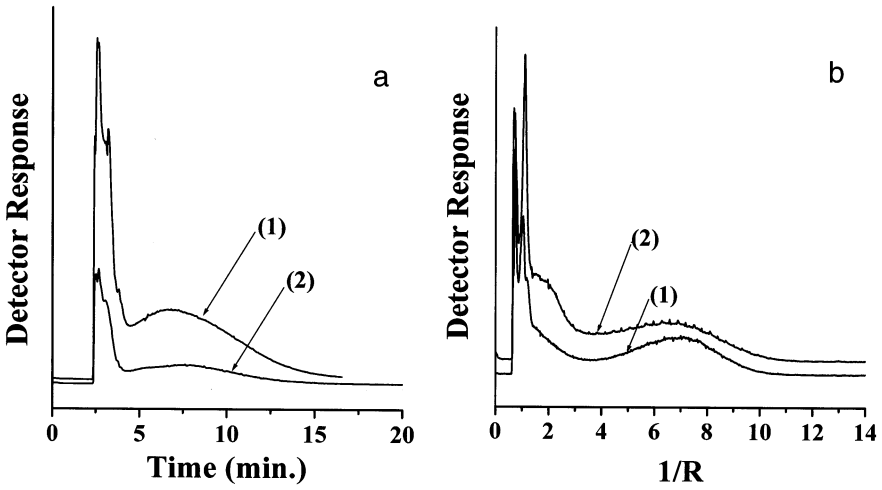

Figure 3. GrFFF of *E. coli.* (a) Fimbriated CS5 0398; sample load, (1) 2.22×10^4 and (2) 0.44×10^4 cells. (b) Nonfimbriated CS5 001101-5; elution flow rate, (1) 0.3 and (2) 0.6 mL min^{-1}.

tometer ($b = 1.0$ cm) was calibrated by using different dilutions of a reference *E. coli* strain of known cell concentration (6.63×10^7 cells mL^{-1}). Regression analysis gives y (UV/visible signal) $= 0.02 \pm 0.01 + (7.6 \pm 0.1) \times 10^{-7} c$ (cells mL^{-1}) ($r = 0.9995$, $N = 15$; $P = 95\%$). The extinction coefficient is 7.6×10^{-7} cm^2 $cells^{-1}$. With this value, the number of cells in each *E. coli* batch was further determined by regression analysis on the same spectrophotometer, with sample dispersions at different cell concentrations. Cell concentration is $(4.44 \pm 0.06) \times 10^7$ and $(7.3 \pm 0.4) \times 10^6$ cells mL^{-1} for the fimbriated CS5 0398 and for the nonfimbriated CS5 001101-5 samples, respectively.

Once the concentration of the *E. coli* batch samples had been determined, the extinction coefficient was evaluated for the UV/visible detector. This allows for fractogram conversion from turbidity signal into number of bacteria. Dispersions of batch samples at different concentrations were fed to the UV/visible detector cell of the workstation BioCAD SPRINT System, and the extinction coefficient was evaluated by regression analysis. The result is $(0.444 \pm 0.004) \times 10^{-6}$ cm^2 $cell^{-1}$. The experimental values of the extinction coefficient are quite different in the detector and in the reference spectrophotometer. This finding could be explained by the known dependence of turbidity measurements on instrument optics, specifically on the acceptance angle.[38]

Once the extinction coefficient for *E. coli* has been determined for the UV/visible detector, it is possible to calculate the number of sorted cells. Determination of the limit of detection of *E. coli* cells by UV/visible turbidity was first performed through flow injection (FIA) of dispersions of fimbriated and nonfimbriated cells at different concentrations. FIA was performed by feeding the injection port directly to the detector via a 30-cm PEEK tube, nominal i.d. 0.050 cm, and by setting the flow rate at the measured value of 0.19 mL min^{-1}. FIA peak area is expected to be proportional to the mass of the injected sample, as described in the literature[38]

$$\bar{A} = (Kb/F)m_0 \qquad (1)$$

where $\bar{A}$ (s) is the area of the turbidimetric FIA peak, m_0 (cells) the number of cells that flow through the detector cell, F the mobile-phase flow rate (mL s^{-1}), and K (cm^2 $cell^{-1}$) is the extinction coefficient. Calibration was then performed by regression analysis on eq 1, which gives $\bar{A} = 0.08 \pm 0.02 + (8.8 \pm 0.3) \times 10^{-5} m_0$. From this regression analysis, the limit of detection is ~2000 *E. coli* cells, which is comparable to the lowest number of bacteria that can be counted by classical methods such as cultivation, and lower than the limit of detection already determined in other types of bacteria by SdFFF−UV/visible spectroscopy.[36]

To assess the ability of UV/visible turbidity to evaluate the fimbriated/nonfimbriated cell ratios, sample mixtures of fimbriated/nonfimbriated cells were run. Such mixtures gave rise to double-band fractograms with different band areas that correspond to different fimbriated/nonfimbriated cell ratios in the injected sample. Panels a and b of Figure 4 show the GrFFF fractograms of two sample mixtures with different fimbriated/nonfimbriated cell ratios. In Figure 4a, the injected numbers of fimbriated (CS5 0398) and nonfimbriated (CS5 001101-5) cells are 5.36×10^4 and 7.64×10^4, respectively, while in Figure 4b, it was, respectively, 1.79×10^5 and 6.62×10^4. It is therefore evident that the fractogram profiles reflect the different amounts of fimbriated/nonfimbriated *E. coli* cells in the mixture. As an example of sorting and quantification of the fimbriated/nonfimbriated ratio in a *E. coli* mixture, Gaussian deconvolution is applied to the digitized GrFFF fractogram in Figure 4a. The fractionated amounts correspond to 1.32×10^5 cells (fimbriated) and 5.77×10^4 cells (nonfimbriated). The totally recovered cells thus are 2.33×10^5. When this latter value is compared to the number of injected cells, the resulting recovery is 95%. Moreover, the recovered ratio of fimbriated/nonfimbriated cells (70:30) is in very good agreement with the known, injected ratio (73:27). High sample recovery and consistency between injected and recovered cell ratio values allow GrFFF−UV/visible spectroscopy to be effectively used for sorting *E. coli*.

AsFlFFF of *E. coli*. The first selectivity studies in reversed AsFlFFF have been performed only very recently.[23] A preliminary

(38) Reschiglian, P.; Zattoni, A.; Melucci, D.; Torsi, G. *Rev. Anal. Chem.* **2001**, *20*, 239−269.

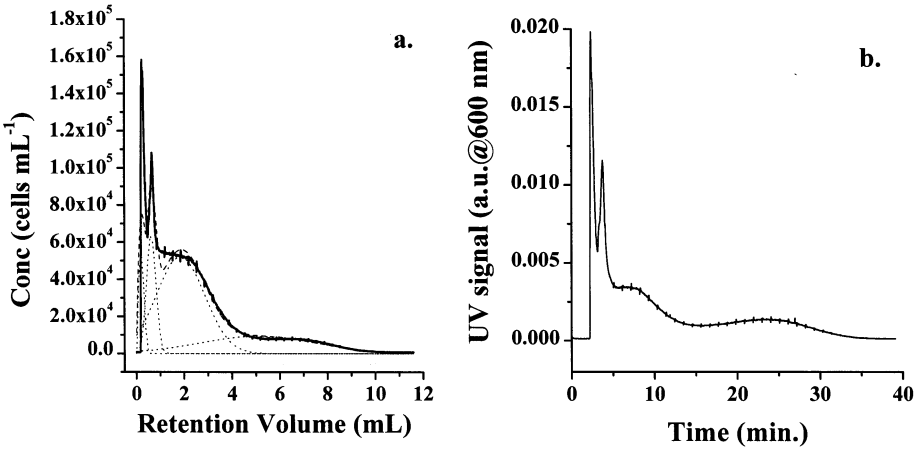

Figure 4. GrFFF−UV/visible spectroscopy of fimbriated CS5 0398/nonfimbriated CS5 001101-5 mixtures. Injected cells, (a) 1.79×10^5 (73%) fimbriated cells, 6.62×10^4 (27%) nonfimbriated cells; recovered cells (fimbriated/nonfimbriated), 70%/30%; total cell recovery, 95%. (b) 5.36×10^4 fimbriated cells/7.64×10^4 nonfimbriated cells.

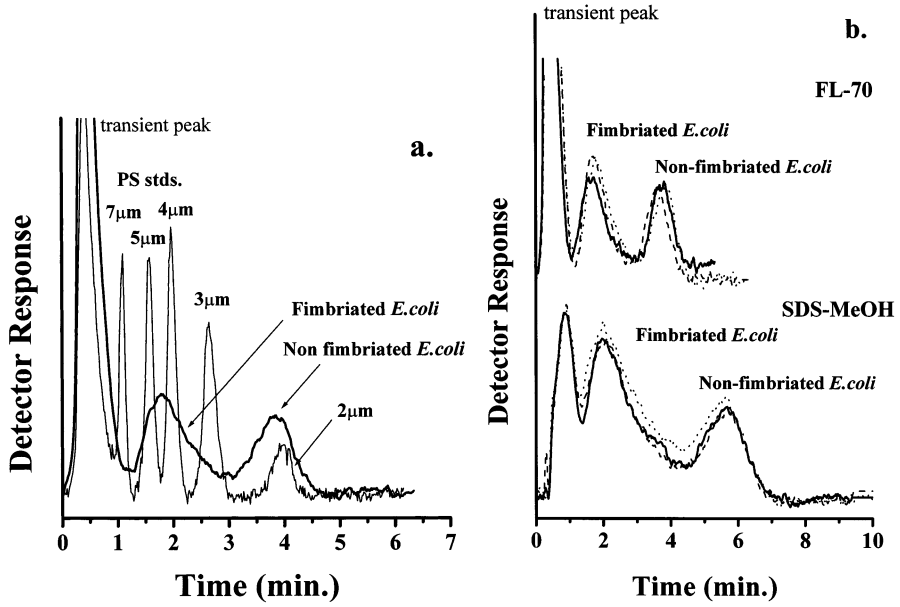

Figure 5. AsFlFFF of fimbriated CS5 0398/nonfimbriated CS5 001101-5 cell mixtures. $V_{out} = 1.3$ mL min^{-1}, $V_{cross} = 0.70$ mL min^{-1}. (a) Comparison with the superimposed separation of a PS mixture. Mobile phase: 0.1% FL-70/0.01% NaN_3. (b) Comparison between retention profiles obtained for different runs with the two carrier solutions: 0.1% FL-70/0.01% NaN_3 and 0.05% SDS/0.01% NaN_3/20% MeOH.

evaluation of the size-based selectivity of the AsFlFFF system here employed for sorting *E. coli* was thus performed with a five-PS mixture (7, 5, 4, 3, and 2 μm). In Figure 5a, one of the repeated runs obtained for the PS mixture at constant $\dot{V}_{out}/\dot{V}_c = 1.3$ mL min^{-1}/0.70 mL min^{-1} is reported. The commonly used mobile phase for FFF of PS was employed (0.1% FL-70/0.01% NaN_3). Separation showed reproducible and at baseline resolution. Analysis time is within 5 min. The very high size-resolving power of AsFlFFF is evident. The elution order of PS in Figure 5a clearly indicates that the elution mode of such micrometer-size beads mixture is reversed. To assess the retention mechanism, a study on PS retention parameters was performed. Relevant data are reported in Table 2, where s_R are the standard deviation values on R, δ (μm) the mean, particle elevation values (defined as $x - d/2$, where x (μm) is the distance of the particle center from the accumulation wall), and γ is the hydrodynamic correction factor value defined as $R/[3(d/w)(1 - d/2w)]$, where w (μm) is the channel thickness. Reproducibility is shown by the low s_R values. The treatment on the lift force contribution toward the retention mechanisms in reversed FFF was given by Williams et al.[39] This model indicates that in Hyp FlFFF δ values must increase with the particle diameter. Values of δ are thus measured as already

Table 2. Retention Parameters for PS Standards in AsFlFFF

sample	diameter (μm)	$R \pm s_R$ ($N = 3$)	δ (μm)	γ
PS 2 μm	2.013	0.162 ± 0.001	2.62	3.51
PS 3 μm	3.004	0.241 ± 0.002	3.98	3.52
PS 4 μm	4.000	0.324 ± 0.0015	5.50	3.56
PS 5 μm	4.991	0.401 ± 0.002	6.94	3.55
PS 7 μm	6.992	0.589 ± 0.002	11.0	3.75

(39) Williams, P. S.; Moon, M. H.; Giddings, J. C. In *Particle Size Analysis*; Stanley-Wood, N. G., Lines, R. W., Eds.; Royal Society of Chemistry: Cambridge, U.K., 1992; pp 280−289.

done for other retention studies in reversed FFF.[23,24,40,41] In Table 2, values of δ are found always higher than the corresponding PS size, and they increase with increasing size. These findings indicate a dominant effect of lift forces on the retention mechanism, and the PS mixture elution in Figure 5a being Hyp AsFlFFF. The corresponding diameter-based selectivity S_d should be then higher than unity. Evaluation of S_d was empirically performed by means of the expression

$$\log t_r = -S_d \log d + \log t_{r1} \qquad (2)$$

where t_{r1} represents the retention time (t_r) of a particle of unit diameter.[34,35,39] The linear regression on the relevant data in Table 2 gives $\log t_r = (0.913 \pm 0.005) - (1.031 \pm 0.006) \log d$ ($r^2 = 0.999$, $N = 15$). Selectivity then is 1.031. Finally, the values of the hydrodynamic factor γ in Table 2 are found to be relatively constant with increasing size and always higher than 2. A value of $\gamma = 2$ is arbitrarily considered to be the boundary between the St/Hyp and Hyp retention mechanism in FlFFF.[34]

Fractionation of mixed fimbriated/nonfimbriated *E. coli* was then carried out in AsFlFFF. The superimposed fractogram in Figure 5a represents the elution of a mixture of fimbriated CS5 0398 and nonfimbriated CS5 001101-5 cells under the same run conditions (the carrier solution and flow rate conditions) employed for the PS mixture. The injected cells were $\sim 8.88 \times 10^4$. The fractogram appears with a huge peak at the beginning of separation. If compared to Figure 4, Figure 5a demonstrates that, with respect to GrFFF, in AsFlFFF, fimbriated cells can be better resolved from the void peak and be baseline separated from nonfimbriated cells, though they are similar in size and shape. Separation time is also shorter in AsFlFFF. By comparing fractograms of nonfimbriated CS5 001101-5, fimbriated CS5 0398, and PS in Figure 5a, one can observe that nonfimbriated cells may be retained in AsFlFFF according to their hydrodynamic radius (see QELS data in Table 1), whereas a significant decrease in retention occurs in the case of fimbriated cells, as observed in GrFFF. Since GrFFF of fimbriated/nonfimbriated cells was performed with a MeOH-added mobile phase (0.05% SDS/0.01% NaN_3/20% MeOH), for better comparison, this organic-modified mobile phase was used also for AsFlFFF. Reproducibility of AsFlFFF of fimbriated/nonfimbriated *E. coli* mixtures was again confirmed by repeated runs. Some of the repeated fractograms are superimposed in Figure 5b. It can be observed that, in AsFlFFF with SDS-MeOH as mobile phase, the band corresponding to fimbriated cells is not completely resolved from the system transient peak (or void peak), although the latter is less intense than in the case with FL-70 as mobile phase. Although FFF−UV/visible signal intensities obtained in different mobile phases cannot be easily compared because of the dependence of UV/visible turbidity response on the dispersing medium,[38] further work showed that the void peak obtained with the mobile phase SDS/MeOH originated from the elution of cell debris or extracellular species possibly present in the fimbriated *E. coli* sample, since injection of single, nonfimbriated cells did not generate such a large void peak. In Figure 5b, retention of both fimbriated and nonfimbriated cells also appears to be increased by the use of the SDS/MeOH mobile phase. This could have been caused by the dramatic increase of mobile-phase viscosity due to the addition of 20% MeOH (at 20 °C, $\eta = 1.604$ cP; $\eta = 1.002$ cP for pure H_2O). It is known that in FlFFF both the hydrodynamic field and lift forces contributions are dependent on viscosity.[42] Dependence of retention on the MeOH content in the mobile phase was first observed by Plockova and Chmelík in GrFFF of silica beads[43] and further confirmed by some of us in GrFFF of PS and yeast cells.[15,16]

To further test size-based sorting capabilities of AsFlFFF for *E. coli*, size-based selectivity studies were performed to establish the elution mode and retention mechanism in AsFlFFF of *E. coli*. Fimbriated and nonfimbriated cells were individually run and collected at narrow time intervals for sizing through FE SEM. In Figure 6a, a fractogram of the nonfimbriated CS5 001101-5 cells obtained with the SDS/MeOH mobile phase is marked in correspondence of the time intervals at which the eluted cells are collected (12 s each). FE SEM pictures of the relevant fractions are also reported in Figure 6a. As mentioned above, injections of single, nonfimbriated cells do not provide a large void peak as observed in Figure 5b but only a negative, system transient peak. The FE SEM measured, average length values of each collected fraction (a_1) are listed in Table 3 a), which shows that the length of nonfimbriated *E. coli* cells decreases as the fraction number increases. This finally confirms, first, that the elution order is reversed also for AsFlFFF of *E. coli* and, second, the excellent size-resolving power of AsFlFFF.

Size-based selectivity was measured for the nonfimbriated cell fractions by means of eq 2. Regression analysis was performed with size values d corresponding to the measured, average length of the rod-shaped cells (a_1) collected at the time interval t_r. Regression equation is $\log t_r = (1.03 \pm 0.02) - (0.87 \pm 0.08) \log a_1$ ($r^2 = 0.970$, $N = 6$). The so-measured S_d value is lower than unity. This finding might indicate a decreased contribution of lift forces on the AsFlFFF retention of *E. coli*, and it also agrees with the increase in retention of *E. coli* observed when such a SDS/MeOH carrier is used (see Figure 5b). However, it must be noted that the mean distance of particle from the accumulation wall (δ), which controls particle separation, significantly varies as the particle deviates from spherical shape, and it is influenced by the nature of the particle motion.[44] The FE SEM-measured, average width values (a_2) for the collected fractions of nonfimbriated *E. coli* cells are reported, for each fraction, in Table 3a. The average a_2 value for all the collected cells is 0.73 ± 0.07 μm, with a corresponding aspect ratio of ~ 2.7. Rod-shaped particles such as *E. coli* cells may thus either roll or tumble end over end while swept down the channel, in response to fluid shear forces. The S_d value of 0.87 for nonfimbriated *E. coli* was in fact obtained for sizes taken as the measured, average length of the cells (a_1). If cell sizes are calculated as the equivalent spherical diameter for each fraction, the size values $d = (3a_2^2a_1/2)^{1/3}$ are in good agreement with the hydrodynamic size determined by QELS (compare data in Table 1 and Table 3a). The regression equation gives, in this case, $\log t_r = (0.94 \pm 0.01) - (2.6 \pm 0.2) \log d$ (r^2

(40) Melucci, D.; Gianni, G.; Torsi, G.; Zattoni, A.; Reschiglian, P. *J. Liq. Chromatogr. Relat. Technol.* **1997**, *20*, 2615−2635.
(41) Reschiglian, P.; Melucci, D.; Torsi, G.; Zattoni, A. *Chromatographia* **2000**, *51*, 87−94.
(42) Williams, P. S.; Moon, M. H.; Giddings, J. C. *Colloid Surf. A* **1996**, *113*, 215−228.
(43) Plockova, J.; Chmelík, J. *J. Chromatogr., A* **2000**, *868*, 217−227.
(44) Beckett, R.; Giddings, J. C. *J. Colloid Interface Sci.* **1997**, *186*, 53−59.

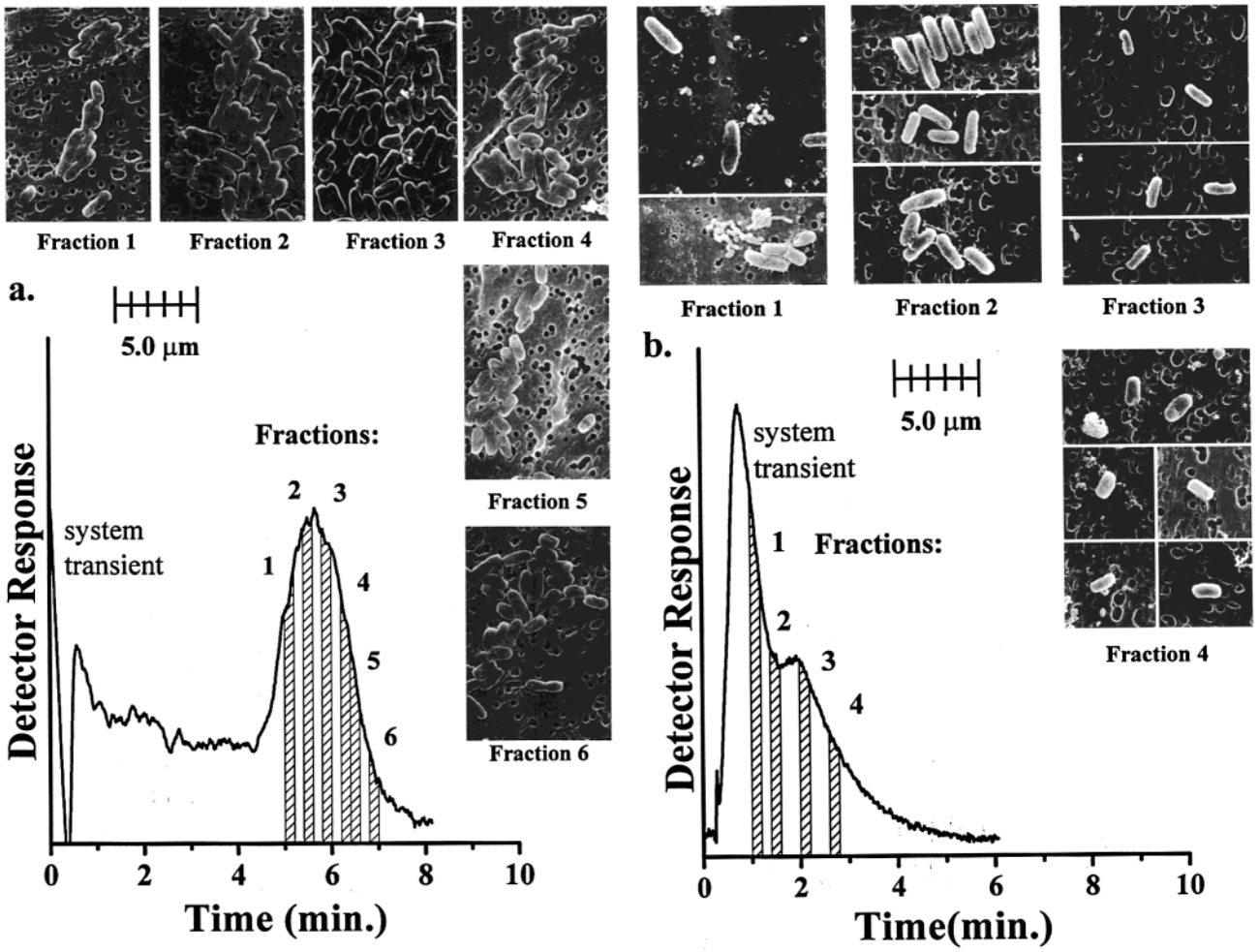

Figure 6. AsFlFFF of *E. coli* with FE SEM micrographs of the collected fractions marked in the fractograms. Mobile phase: 0.05% SDS/0.01% NaN_3/20% MeOH; $V_{out} = 1.3$ mL min^{-1}, $V_{cross} = 0.70$ mL min^{-1}. (a) Nonfimbriated CS5 001101-5; (b) fimbriated CS5 0398.

Table 3. Measured Average Length and Width of *E. coli* Cells in AsFlFFF Fractions Collected in Figure 6a,b[a]

N fractions[a]	time (min)	length (a_1) (μm)	width (a_2) (μm)	equivalent d (μm)[b]
(a) Nonfimbriated CS5 001101-5				
1 ($n = 40$)	5.0−5.2	2.32 ± 0.51	0.65 ± 0.11	1.22
2 ($n = 40$)	5.4−5.6	2.18 ± 0.43	0.71 ± 0.07	1.20
3 ($n = 40$)	5.8−6.0	2.02 ± 0.30	0.72 ± 0.08	1.17
4 ($n = 40$)	6.2−6.4	1.93 ± 0.36	0.74 ± 0.06	1.15
5 ($n = 40$)	6.4−6.6	1.76 ± 0.35	0.73 ± 0.07	1.11
6 ($n = 40$)	6.8−7.0	1.66 ± 0.28	0.73 ± 0.07	1.09
(b) Fimbriated CS5 0398				
1 ($n = 40$)	1.0−1.2	2.13 ± 0.42	0.65 ± 0.08	1.11
2 ($n = 40$)	1.4−1.6	1.79 ± 0.32	0.63 ± 0.07	1.02
3 ($n = 10$)	2.0−2.2	1.67 ± 0.42	0.59 ± 0.10	0.955
4 ($n = 10$)	2.6−2.8	1.44 ± 0.13	0.67 ± 0.09	0.990

[a] *n*, number of counted cells. [b] Equivalent spherical diameter, $d = (3a_2^2a_1/2)^{1/3}$.

$= 0.970$, $N = 6$). Selectivity is much higher ($S_d = 2.6$) than in the previous case, $d = a_1$, since size polydispersity is apparently reduced when cell size values are determined as the equivalent spherical diameter, as shown in Table 3a. From the relevant S_d values, nonfimbriated cells thus appear to elute as though they were spheres of diameter equal to the cell length rather then spheres of equal volume.

In Figure 6b, the fractogram of fimbriated CS 50398 cells is also marked in correspondence of the time intervals at which the eluted cells were collected (12 s each). FE SEM micrographs for sizing the relevant fractions are also reported in Figure 6b. As in Figure 5b, Figure 6b shows a large void peak caused by cell debris (extracellular matter), the presence of which is shown in the FE SEM micrographs of fraction 1. The void peak is however more intense than in Figure 5b, where the sample is in fact a mixture of fimbriated and nonfimbriated cells that, when injected alone, give a negative transient peak (see Figure 6a). Because of the bigger overlap with the void peak, fimbriated cells in Figure 6b seem to be less retained than in Figure 5b, which does not show the true case. In fact, when the mixture of fimbriated and nonfimbriated cells is injected (Figure 5b), the huge void peak caused by the elution of extracellular species of the fimbriated *E. coli* sample is offset by the negative response of the void peak region for nonfimbriated cells. This results in the decrease of the void peak for the mixture, which then leads to the isolation of the resolved peak for fimbriated *E. coli*. From FE SEM micrographs of Figure 6b, the presence of extracellular matter is also shown in more retained fractions, and it could have originated from detachment of fimbriae from the bacterial membrane.

It is worth noting that AsFlFFF retention order is reversed for the fimbriated cells as well, with retention increasing with

decreasing cell length. Dimensions of the fimbriated cells in the collected fractions are reported in Table 3b. Average length and width values were similar to those measured for the nonfimbriated cells. Nonetheless, retention of fimbriated *E. coli* in Figure 6b is significantly reduced with respect to that expected from their size. According to the reversed elution mode, it means that fimbriated cells behave as though they were of larger size. This finding supports the suggestion that fimbriae could play a role in lifting cells by making fimbriated cells behave as if they were bigger particles. When regression analysis for measuring S_d is performed with fimbriated cells and the measured cell length is used for size (i.e., $d = a_1$), the result would be $\log t_r = (0.82 \pm 0.08) - (2.4 \pm 0.3) \log d$ ($r^2 = 0.983$, $N = 4$). The measured size-based selectivity for fimbriated cells is thus much higher ($S_d = 2.4 \pm 0.3$) than that of nonfimbriated cells ($S_d = 0.87 \pm 0.08$). This abnormally high S_d value for fimbriated cells is not statistically different from the value calculated for nonfimbriated *E. coli* when cells were considered as spheres of volume equal to the cell volume ($S_d = 2.6 \pm 0.2$). This surprising agreement between the S_d values should support the fact that fimbriated *E. coli* cells in AsFlFFF behave as larger particles of broader polydispersity. It must be recalled that in FFF the extent of the size polydispersity contribution to plate height is related to the size-based selectivity.[2] Fimbriae protrusion from the cell membrane may explain the apparent increase in cell size and size polydispersity.

CONCLUSIONS

GrFFF and AsFlFFF have been shown to be effective for sorting bacteria strains of the same species. Each technique displays its own features, which can be of specific interest for selected applications. GrFFF is low cost and it can be easily implemented in a standard HPLC system by only the substitution of the column. The channel can be homemade with minimal machine shop work. Part of the GrFFF work described in this paper was performed at SBL Vaccin. SBL laboratories had no previous experience of FFF. The channel had been previously assembled elsewhere and then plugged in a standard HPLC workstation. First *E. coli* fractograms were obtained after a trial period that required less than 48 h. Once the GrFFF work had been finished, the HPLC workstation was ready to return to standard HPLC operations. These GrFFF features should make it possible for nonspecialized laboratories to perform bacteria sorting by means of standard HPLC expertise and minimal investments. AsFlFFF showed excellent sorting performance at very short analysis time and very high size-based selectivity. Size-based selectivity studies allowed for the analysis of the retention mechanism for an interpretation of the experimental fact that nonmotile *E. coli* cells of similar size and shape can be baseline separated even if they differ only in surface characteristics (i.e., the presence of fimbriae).

All the above points are fundamental for the assessment of bacteria sorting methods based on FFF. If compared to other methods, the FFF techniques employed here show prime advantages. They are, first, separation methods. No other flow-assisted separation methods are currently available for bacteria sorting based on differences in surface characteristics. Flow cytometry is widely applied to sort and characterize cells. However, its application to bacteria requires high-intensity light sources and long analysis time, and the instrumental cost of flow cytometers cannot be compared to that of FFF systems. Other techniques for the analysis of morphological and surface features of bacteria are available. In most cases, they are based on immunoreactions but they are not separation techniques. Hemoagglutination and colony lift hybridization can, in fact, differentiate between fimbriated and nonfimbriated cells, but they are time-consuming and nonquantitative techniques. UV/visible turbidity is shown here to be capable of adding a quantitative, accurate response to the sorting capabilities of FFF. Electron microscopy is accurate in sizing and displaying bacterial surface features. However, it is expensive and also time-consuming. Otherwise, QELS gives size but no information on bacterial surface features.

In this work, FFF−UV/visible spectroscopy has been employed for sorting deactivated bacteria. However, when biocompatible buffers are used as mobile phases, preliminary work shows that plastic channels and membranes used in FFF are biocompatible for sorting live bacteria and cells. Further work is on progress and it may be the object of further papers. FFF−UV/visible spectroscopy eventually shows its potential in bacteria sorting in the area of various microbiology and biomedical, pharmaceutical, diagnostic, food, and environmental fields.

ACKNOWLEDGMENT

This work was supported by research grants of the University of Bologna and Pusan National University and by Leonardo-EXCHANGE 2001 between the University of Bologna, and SBL Vaccin AB, a financial program for researchers' mobility from the university to small and medium enterprises within UE.E. Whitmore-Carlsson, SBL Vaccin AB is duly acknowledged for accurate details on sample specifications and helpful discussion. Thanks also goes to M. Guardigli, University of Bologna, for QELS measurements, to C. Scala, University of Bologna for sample preparation for SEM, and to Ph.J.P. Cardot, University of Limoges (France), for his help on GrFFF instrumental developments. Part of this work was presented at FFF 2001, 9th International Symposium on Field-Flow Fractionation, Golden, CO, June 26−29, 2001.

Received for review March 26, 2002. Accepted July 16, 2002.

AC020199T